

Predominance Diagrams of Spent Nuclear Fuel Materials in LiCl-KCl and NaCl-KCl Molten Salt Eutectics

Rema Abdulaziz, Leon D. Brown, Douglas Inman, Stefaan Simons, Paul R. Shearing and Daniel J. L. Brett*

Electrochemical Innovation Lab, Department of Chemical Engineering, University College London, Torrington Place, London, WC1E 7JE, United Kingdom

*E-mail: d.brett@ucl.ac.uk

Received: 27 April 2016 / Accepted: 25 September 2016 / Published: 10 November 2016

Predominance phase diagrams for metal-molten salt systems are diagrams of potential vs. the negative logarithm of the activity of O^{2-} ions ($E-pO^{2-}$); they are a valuable tool for predicting and understanding electrochemical systems and for optimising process conditions. Here, predominance diagrams are produced for the range of nuclear spent materials (U, Pu, Np, Am, Cm, Cs, Nd, Sm, Eu, Gd, Mo, Tc, Ru, Rh, Ag and Cd species), in both LiCl-KCl at 500 °C and NaCl-KCl at 750 °C. The two salt eutectics were chosen as they are the two main systems used for pyroprocessing; temperatures were selected within each salts normal operating range. All of the diagrams presented show regions of stability for the different metal species, their oxides and chlorides at unit activity; however, this activity can be altered in accordance with the equations derived. Examples of selective electrochemical reduction are also demonstrated for potential spent fuel reprocessing in both salt systems.

Keywords: Predominance diagrams; Spent fuel; Nuclear materials; Molten salts; Pyroprocessing.

1. INTRODUCTION

Nuclear energy for electricity generation offers large-scale low-carbon energy production, but suffers with challenges such as the handling of waste materials. Reprocessing of spent nuclear fuel significantly reduces the greenhouse gas emissions associated with the nuclear fuel cycle, and reduces the burden on waste storage [1]. While the reprocessing of some of the spent fuel materials increases the efficiency of the fuel-cycle, the reprocessing of other materials, such as the minor actinides, is important for public acceptance of civilian nuclear power.

1.1. Pyroprocessing

Reprocessing of spent nuclear fuel was first carried out in the 1940s for the separation of Pu species for military purposes and applied to U in civilian power generation. More recently, reprocessing of irradiated fuel is used in facilitating the disposal of high-level nuclear waste.

Pyrochemical processing or pyroprocessing is a non-aqueous high-temperature electrochemical method for the refinement and separation of irradiated spent nuclear fuel. Pyroprocessing is generally a desired scheme as it employs compact facilities, which are economically favourable for decontamination, and it also requires a shorter cooling period for irradiated fuel. Different process schemes and salts have been studied in pyroprocessing, most of which have been summarised by the Nuclear Energy Agency (NEA) [2]. There are currently two main molten salt technology processes in existence, both using chloride salts as electrolytes; one in the US at the Argonne National Laboratory (ANL) using LiCl-KCl eutectic, for metallic fuel in Integral Fast Reactors (IFR), and one in Russia at the Research Institute for Atomic Reactors (RIAR) using NaCl-KCl eutectic, for oxide fuel for Fast Breeder Reactors (FBR) [3]. There have also been other advances made in molten salt nuclear pyroprocesses in Europe and Japan [4-9].

1.2. Predominance diagrams

Predominance diagrams (also known as Littlewood diagrams) were originally developed by Littlewood in 1962 [10] to summarise thermodynamic characteristics of metal-molten salt systems and are akin to Pourbaix diagrams, which describe the behaviour of species in aqueous solutions. In Pourbaix diagrams, the equilibrium potential is plotted against pH to show regions of stability for a specific metal-aqueous solution system [11]. Whereas predominance diagrams show potential vs. the negative logarithm of the activity of oxygen anions: the pO^{2-} .

The fundamental notion of predominance diagrams is to represent thermodynamic data in a diagrammatic form. Data is converted to linear equations relating free energies to logarithmic functions of material composition. The free energies of the system are represented by potentials that are relative to the electrochemical equilibrium between the salt's anion and its elemental form, in chloride salts this is the standard chlorine electrode. The composition variable is the negative logarithm of the activity of the oxygen ions in the melt, pO^{2-} (analogous to pH). These diagrams are very useful when studying complex metal-molten salt systems, such as Li-K-U-O-Cl, as they describe the regions of stability and the pathways of the system's evolution at different equilibrium potentials.

The procedure for producing predominance diagrams is best described in the works of Littlewood, Dring *et al.* and Brown *et al.* [10, 12, 13]. Predominance diagrams have been developed for various systems [14-21], providing valuable insight into the electrochemical processes of metals and their oxides in molten salts. However, they are not flawlessly accurate, fundamentally predominance diagrams are only as accurate as the thermodynamic data used to create them, and therefore they need to be validated experimentally, as reaction kinetics and surface processes will have a dominant effect in defining reaction rate. Extensive work has been performed to characterise the reduction of TiO_x in CaCl [22]; this has been compared with the predominance diagram produced by

Dring *et al.* [12]. X-ray diffraction analysis of the reduction process of TiO_x at different stages has been carried out by Schwandt and Fray, Wang and Li, and Bhagat *et al.* [23-25], providing validation of processes predicted by the predominance diagram.

According to Le Chatelier's principle, the change in operating conditions during a process results in shifts in equilibria. Hence, other issues could arise due to the solubility of some oxide species in the melt and the evaporation of some chloride species. This would shift the operating equilibria away from the predicted ones on the predominance diagrams [12].

Another limitation is that there is no adequate experimental technique for keeping the O^{2-} levels within a specified limit. Studies have looked at monitoring and controlling the $p\text{O}^{2-}$ in molten salts [26]; but it is very difficult to implement in practice, particularly on a larger scale. Rigorous salt preparation can reduce the O^{2-} ions concentration; however, once the reduction of a metal oxide proceeds, the increase of O^{2-} concentration in the melt shifts the equilibrium potential. Also, the degradation and the formation of pores on the working electrode can act to 'trap' O^{2-} ions, thus increasing the levels at the interface, changing the regions of stability in the diagrams again. New reactor cell designs could prove useful here, such as the fluidised cathode process [27], as it would help disperse the O^{2-} ions, and give the system more homogeneity.

The nuclides commonly considered in burn-up credit analysis by the NEA [28] are shown in Table 1. It also lists their half-lives, their content (in g per metric tonne of heavy metal, g/MTHM) in uranium oxide (UOX) pressurised water reactor (PWR) spent-fuel and their relative importance according to the NEA. Different nuclides of uranium and plutonium are of highest importance, and their content in spent-fuel is significant. All of these nuclides are classed as high-level waste.

In this article, the authors produce predominance diagrams for spent nuclear materials in LiCl-KCl eutectic at 500 °C, as is in use at the ANL, and NaCl-KCl eutectic at 750 °C, as is in use at the RIAR. The temperatures were chosen to be within the salts' common operating temperature ranges [3, 29].

Table 1. List of nuclides commonly considered in burn-up credit criticality analyses (from NEA 2011) [28] and used as the basis for the systems examined here.

Nuclide	Half-life (years)	Content in spent UOX PWR fuel ^a (g/MTHM) 52 GWd/t at discharge	Relative importance rank for 40 GWd/MTHM PWR fuel – 5 years cooling ^b
²³⁴ U	2.45×10^5	143	24
²³⁵ U	7.04×10^8	6050	1
²³⁶ U	2.34×10^7	5650	11
²³⁸ U	4.47×10^9	927000	3
²³⁸ Pu	87.74	372	22
²³⁹ Pu	2.41×10^4	5810	2
²⁴⁰ Pu	6550	2840	4
²⁴¹ Pu	14.40	1820	5
²⁴² Pu	3.76×10^5	1020	19
²³⁷ Np	2.14×10^6	811	14

²⁴¹ Am	432.60	228	10
²⁴³ Am	7370	1.74	11
²⁴³ Cm ^c	28.50	0.624	
²⁴⁴ Cm ^c	18.11	141	
²⁴⁵ Cm ^c	8532	11	
¹³³ Cs	Stable	1630	12
¹⁴³ Nd	Stable	1070	7
¹⁴⁵ Nd	Stable	989	17
¹⁴⁷ Sm	1.06×10^{11}	196	20
¹⁴⁹ Sm	2.00×10^{15}	3.36	6
¹⁵⁰ Sm	Stable	446	23
¹⁵¹ Sm	93	14.7	9
¹⁵² Sm	Stable	134	15
¹⁵³ Eu	Stable	184	18
¹⁵⁵ Gd	Stable	3.93	13
⁹⁵ Mo	Stable	1180	21
⁹⁹ Tc	2.10×10^5	1120	16
¹⁰¹ Ru	Stable	1210	26
¹⁰³ Rh	Stable	540	8
¹⁰⁹ Ag	Stable	119	25
¹¹³ Cd ^c	9.10×10^{15}		

^a Measured content from ARIANE experimental programme data.

^b Based on relative sensitivity coefficients from the Nuclear Regulatory Commission (2008) [30].

^c Important for MOX fuel only.

2. THEORY

To construct a predominance diagram, one needs to employ the following equations and follow the subsequent steps. The standard Gibbs energy of formation of a given reaction, ΔG , may be related to the electrochemical potential of the specific cell, E , by Equations 1 and 2, and by the Nernst Equation 3. In these equations, n is the moles of electrons transferred in a reaction, F is Faraday's constant ($96485.4 \text{ C mol}^{-1}$), R is the universal gas constant ($8.314 \text{ J mol}^{-1} \text{ K}^{-1}$), T is the operating temperature of the molten salt in Kelvin, and Q is the reaction quotient.

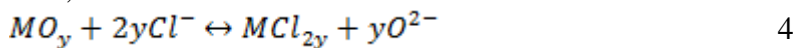
$$\Delta G^\circ = -nFE^\circ \quad 1$$

$$\Delta G = -nFE \quad 2$$

$$E = E^\circ - \frac{RT}{nF} \ln Q \quad 3$$

The potential window of the salt defines the bounds of the predominance diagram. For example, in LiCl-KCl, Cl_2 gas evolution defines the oxidative limit, and formation of metallic Li or K defines the reductive limit. The oxidative limit (in this example, the formation of Cl_2) is assigned a Gibbs energy of formation of zero, at all temperatures, to maintain a zero potential reference point. This is when the Cl_2 formed is at unit activity with the Cl^- ions in the melt at one atmospheric partial pressure. From this zero reference point, the regions of stability for the system chosen extend to the reductive limit, the decomposition potential of the salt.

There are three types of equilibrium that define the thermodynamic regions of stability for a specific species: one that does not involve transfer of electrons; one that does not involve transfer of oxide anions; and one that depends on both electron and oxide anions being transferred. Reactions 4, 5 and 6 represent the three kinds of equilibrium, where M is metal. Using Equations 1, 2 and 3, the equations in terms of electrode potential, E , and pO^{2-} , for each reaction can be derived, as seen in Equations 7, 8 and 9.



$$pO^{2-} = \frac{\Delta G_4^0 + RT \ln \left(\frac{a_{MCl_{2y}}}{a_{MO_y}} \right)}{yRT \ln 10} \quad 7$$

$$E_5 = \frac{-\Delta G_5^0}{nF} - \frac{RT}{nF} \ln \left(\frac{a_{M^z}}{a_{M^{z+n}}} \right) \quad 8$$

$$E_6 = \frac{-\Delta G_6^0}{nF} - \frac{RT}{nF} \ln \left(\frac{a_{MO_{x-y}}}{a_{MO_x}} \right) + \frac{yRT \ln 10}{nF} pO^{2-} \quad 9$$

Predominance diagrams for metal-molten salt systems are generally divided into three main regions of stability, where different species exist: one where the pure metal exists, either in the salt solution or precipitates as a solid; one where the metal is covered by an oxide layer or is fully oxidised, also as a solute in the liquid salt or a solid species; and one where the metal is in the form of a chloride, liquid or gas [10]. This is illustrated in Figure 1.

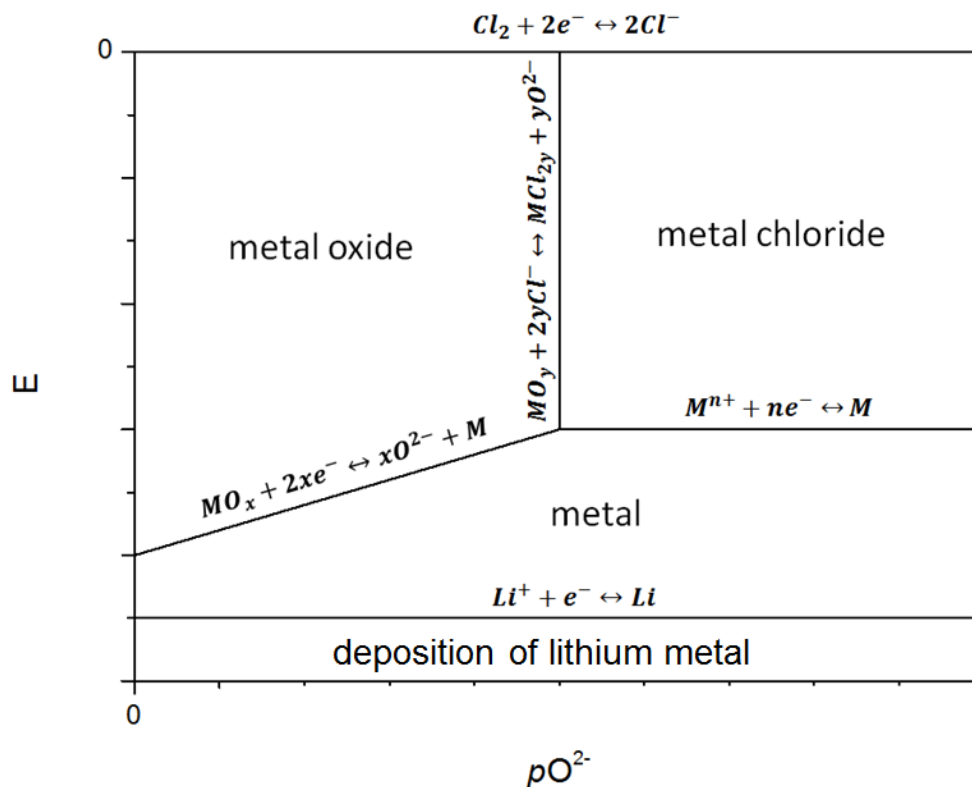


Figure 1. Example of the three main regions of stability in a predominance diagram (based on a LiCl-KCl salt eutectic) and showing the nature of reactions leading to horizontal, vertical and diagonal lines

The limiting potentials for the salt, at any given partial pressure of chlorine gas, and activity of liquid lithium metal and liquid potassium metal, may be calculated according to their corresponding Nernst Equations. For the LiCl-KCl electrolyte at 500°C, the potentials are solid horizontal lines at 0 V, -3.57 V and -3.76 V for the evolution of Cl₂, Li and K respectively; and for the NaCl-KCl eutectic at 750 °C, and the potentials for the evolution of Na and K were found to be -3.28 V and -3.52 V respectively.

The next step is to calculate the Gibbs energy of formation of an oxide ion in the melt. There are two standard states for the oxide ion in the salt eutectic, these are Li₂O and K₂O. At 500°C, the Gibbs energy of formation for O²⁻ from its standard state Li₂O is +191.71 kJ mol⁻¹, and that from the standard state K₂O is +469.32 kJ mol⁻¹. The salt in this system is a LiCl-KCl eutectic with a molar composition of 59-41 respectively. Therefore, the Gibbs energy of formation for the oxide ion at 500 °C in this system is +305.56 kJ mol⁻¹. The same method was applied to the NaCl-KCl equimolar system at 750 °C, and the Gibbs energy of formation for the oxide ion in the molten salt was established to be +408.91 kJ mol⁻¹.

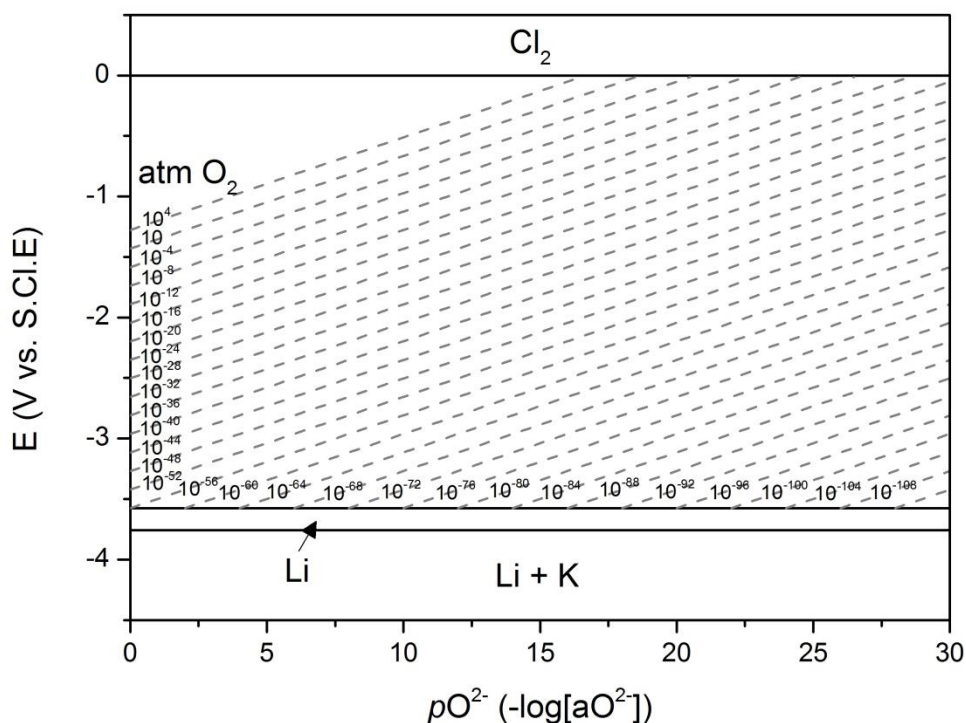


Figure 2. Predominance diagram for the Li-K-O-Cl system at 500 °C, illustrating the relationship between oxygen pressure, oxide activity and potential, *E*, relative to the standard chlorine electrode

Moreover, oxygen anions are in equilibrium with the atmosphere. Using the Gibbs energy of formation for O²⁻ and the Nernst equation, Equation 10 can be derived.

$$E_{O^{2-}} = E_{O^{2-}}^{\circ} + \frac{RT \ln 10}{4F} \log P_{O_2} + \frac{RT \ln 10}{2F} pO^{2-} \tag{10}$$

This shows the relationship between the electrode potential as a function of standard state potential, the oxygen gas partial pressure and the negative logarithm of the oxide ion activity, pO^{2-} . It is depicted in the predominance diagram, in Fig. 2, as a series of diagonal dashed lines, showing several states of equilibrium between oxygen gas and oxide ions, at various O_2 partial pressures. The information from this diagram is very useful for molten salt systems, where partial pressures of oxygen are normally very low, as it shows the potentials at which O_2 would be in equilibrium with the melt. These lines can be derived for the NaCl-KCl eutectic system following the same procedure. They can be superimposed onto the metal phase diagrams; however, to aid visual interpretation this is not performed here.

The functions of the interface lines between the different regions of stability, for each system, were derived using Reactions and Equations 4-9 and the thermodynamic data presented in Table 2. Pure liquid phases were assigned an activity of unity and pure gases were assigned unit atmosphere partial pressure. The diagrams depict regions of stability for species in solution and solid phases that would precipitate out, as well as liquid and gas phases. These diagrams can also be altered, by changing the activity used and conditions, which would shift the equilibria lines accordingly. For simplicity, unit activities are shown here. The predominance diagrams for the spent nuclear fuel materials in LiCl-KCl eutectic at 500 °C and NaCl-KCl eutectic at 750 °C are presented in Fig. 3-6.

Table 2. Gibbs energy of formation for nuclear materials at 500 and 750 °C.

Species	ΔG_f^0 (kJ mol ⁻¹) at 500 °C	ΔG_f^0 (kJ mol ⁻¹) at 750 °C	Comments	References
LiCl (NaCl at 750 °C)	-344.887	(-316.766)		[31-33]
Li ₂ O (Na ₂ O at 750 °C)	-498.105	(-274.608)		[31, 34-38]
KCl	-362.418	-339.473		[39, 40]
K ₂ O	-255.559	-220.057		[34, 35]
Li ₂ UO ₄ (Na ₂ UO ₄ at 750 °C)	-1662.680	(-1486.881)	Extrapolated above 27 °C	[37, 38, 41]
UO	-477.980	-455.771	Extrapolated above 227 °C	[42]
UO ₂	-950.563	-907.756		[35, 43]
U ₄ O ₉	-3921.203	-3736.848		[35]
U ₃ O ₈	-3055.659	-2896.089		[35]
UO ₃	-1023.699	-962.404		[31, 34, 35]
UCl ₂ O	-888.723	-837.432	Extrapolated above 527 °C	[36, 41]
U ₂ Cl ₅ O ₂	-1796.568	-1677.069	Extrapolated above 427 °C	[37]
UCl ₃	-692.619	-642.160		[37, 41]
UCl ₄	-794.542	-735.413		[31, 44]
Pu ₂ O ₃	-1475.278	-1410.029		[34, 35]
PuO ₂	-908.526	-861.327		[34-36]
PuClO	-806.625	-765.969		[41, 43]
PuCl ₃	-787.684	-733.376		[40, 41, 44]
Li ₂ NpO ₆ (Na ₂ NpO ₄ at 750 °C)	-1355.089	(-1346.466)	Extrapolated above 27 °C	[38]
NpO ₂	-938.781	-894.564		[35, 41]

Np ₂ O ₅	-1822.103	-1709.164	Extrapolated above 527 °C	[41]
NpCl ₃	-725.188	-670.084		[41, 43]
NpCl ₄	-758.434	-705.146	Extrapolated above 727 °C	[41]
Am ₂ O ₃	-1473.270	-1406.104		[41]
AmO ₂	-795.968	-756.153		[33, 41]
AmClO	-817.211	-777.668		[41]
AmCl ₃	-795.282	-739.928	Extrapolated above 27 °C	[41]
Cm ₂ O ₃	-1430.229	-1328.186	Extrapolated above 27 °C	[45]
CmO ₂	-748.492	-684.109	Extrapolated above 27 °C	[45, 46]
CmClO	-807.035	-744.292	Extrapolated above 27 °C	[45]
CmCl ₃	-767.028	-683.871	Extrapolated above 27 °C	[45]
Cs ₂ O	-242.961	-205.878		[34, 44]
Cs ₂ O ₂	-283.880	-228.116		[34, 42, 44]
Cs ₂ O ₃	-327.724	-259.383	Extrapolated above 427 °C	[36]
CsO ₂	-173.900	-136.486	Extrapolated above 200 °C	[37]
Nd ₂ O ₃	-1587.405	-1519.064		[34, 35, 37]
NdO ₂	-696.669	-447.885	Extrapolated above 200 °C	[47]
NdClO	-855.745	-811.395		[31]
NdCl ₃	-852.695	-796.445		[37]
Sm ₂ O ₃	-1597.552	-1524.838		[31, 35]
SmClO	-861.226	-817.884	Extrapolated above 727 °C	[37]
SmCl ₃	-838.055	-783.450		[31, 44]
EuO	-513.126	-489.177		[34, 37, 44]
Eu ₂ O ₃	-1409.857	-1335.566		[37]
EuClO	-750.346	-703.088		[42]
EuCl ₃	-737.401	-683.034		[37, 44]
Gd ₂ O ₃	-1615.765	-1545.666		[34, 43, 44]
GdClO	-841.390	-797.533	Extrapolated above 727 °C	[31, 33, 34]
GdCl ₃	-815.177	-765.475	Extrapolated above 727 °C	[36, 44]
Li ₂ MoO ₄ (Na ₂ MoO ₄ at 750 °C)	-1232.046	(-1086.773)		[35, 37, 40, 48]
MoO ₂	-445.688	-402.174		[35, 38, 49]
MoO ₃	-547.974	-487.662		[31, 34, 35]
MoCl ₂ O	-357.355	-305.131		[33, 34]
MoCl ₂	-172.364	-136.825		[33, 34, 37]
MoCl ₅	-284.750	-223.078		[32, 44]
TcO ₂	-314.411	-270.073		[36, 41]
TcO ₃	-349.485	-300.478	Extrapolated above 127 °C	[31]
Tc ₂ O ₇	-738.443	-644.378	Extrapolated above 427 °C	[35, 40]
TcCl ₃	-133.223	-88.864		[42]
RuO ₂	-172.921	-133.825		[36]
RuO ₄	-47.246	0.188	Extrapolated above 172 °C	[37]
RuCl ₃	-54.551	-4.138	Extrapolated above 450 °C	[36]
Rh ₂ O	-57.798	-47.534	Extrapolated above 727 °C	[43]

RhO	-31.229	-13.954		[43]
RhCl	-40.413	-28.786		[42]
RhCl ₂	-65.752	-41.129		[42]
RhCl ₃	-92.650	-39.953		[36-38]
Ag ₂ O	19.033	33.200		[33, 37, 45]
AgO	55.057	76.216	Extrapolated above 125 °C	[46]
Ag ₂ O ₃	286.073	386.987	Extrapolated above 125 °C	[45]
AgCl	-86.475	-80.450		[33, 37, 38]
CdO	-181.481	-155.461		[37, 38, 43]
CdCl ₂	-270.663	-240.187		[33, 36]

3. RESULTS

Some of the general features of the predominance diagram can be illustrated by reference to the uranium system in Fig. 3 (a). Compounds with uranium at their highest oxidation states are found in the upper regions of the diagram, at less negative potentials. At very low oxide ion activities, on the right hand side of the diagram, uranium chlorides (UCl₃, UCl₄) are formed. Uranium metal can be extracted from these at less negative potentials compared to the reduction of UO₂. Since there is no transfer of O²⁻ ions in these reactions, from U⁴⁺ to U³⁺ and to U, the resultant interline functions between these species' regions of stability are independent of pO^{2-} . Thus, the interfaces are represented as horizontal lines in the predominance diagram.

Due to the stability of other compounds that could exist in the melt, there is an intermediate region of stability between the oxides and the chlorides. This intermediate region is in the metal oxychloride form. In the case of uranium it is UCl₂O and U₂Cl₅O₂. The interface between these two phases is a horizontal line, as there is no transfer of O²⁻ occurring. The interfaces between the regions of stability of the reactions from UO₂ to UCl₂O and to UCl₄ are all vertical lines; hence, the derived interface equations are independent of potential. All the other equations for interface lines related to UCl₂O and U₂Cl₅O₂ are dependent on both pO^{2-} and E , resulting in diagonal lines.

At high oxide ion activities, on the left hand side of the predominance diagram, other types of uranium oxides are predicted to form. This is due to the oxide ions reacting with lithium or potassium in the fused salt. In the case of uranium, the first stable metal uranium oxide to form is Li₂UO₄, as presented in Fig. 3 (a).

For the electrochemical reduction of UO_x to U metal, the reductive potential is very negative and close to the salt's decomposition potential. The diagram gives an indication of the number of phases expected to appear, and the order they would appear in, if UO₃ was to be reduced. It can also be deduced that some compounds, such as U₃O₇, UO and U₄O₉, have a very narrow band of stability, when reducing the uranium oxide; thus, it is not very likely that traces of them will remain in the final product, as is the case with TiO_x [25].

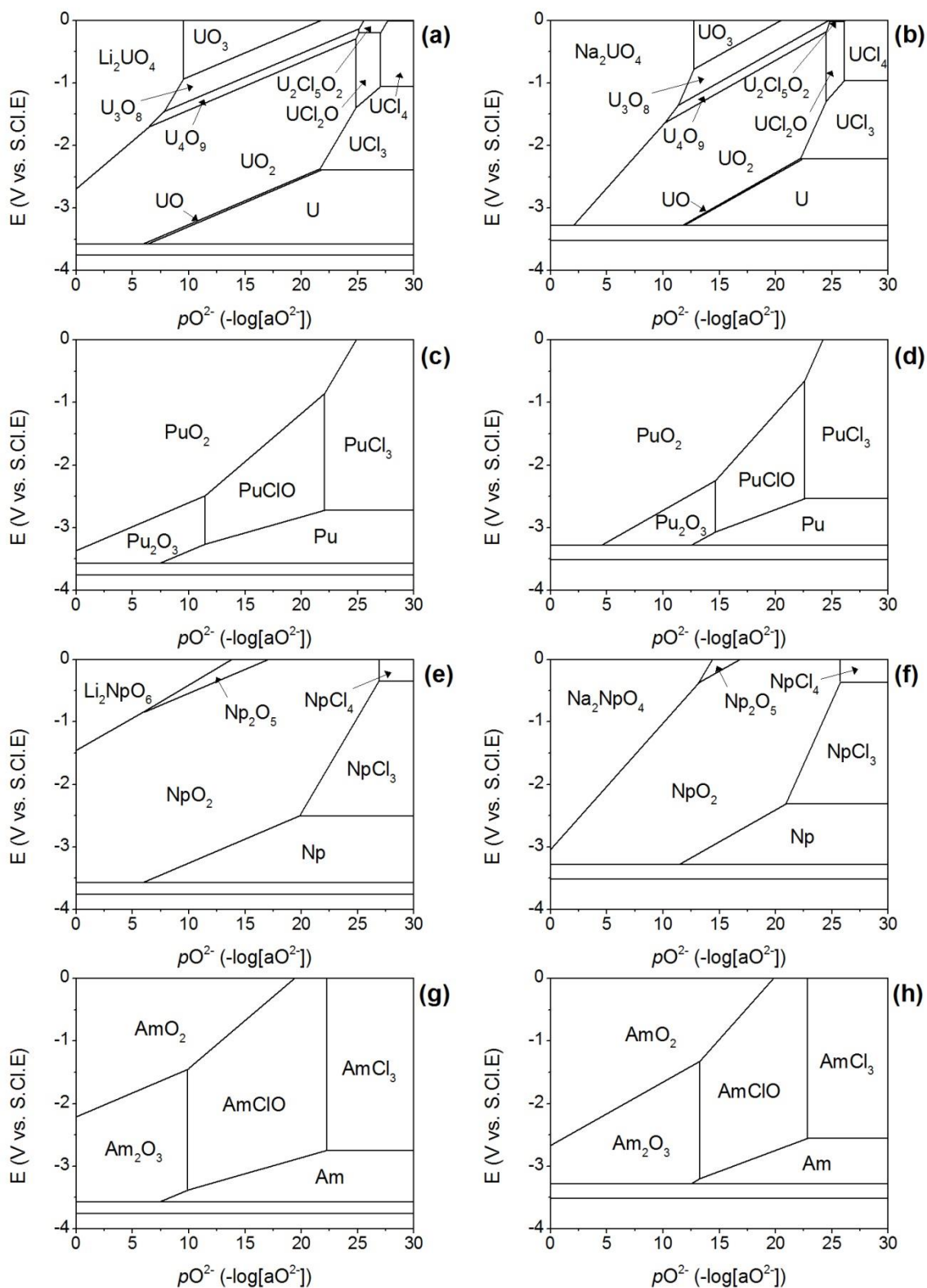


Figure 3. Predominance diagrams of (a) U, (c) Pu, (e) Np, and (g) Am in LiCl-KCl at 500 °C. (b) U, (d) Pu, (f) Np, and (h) Am are in NaCl-KCl at 750 °C

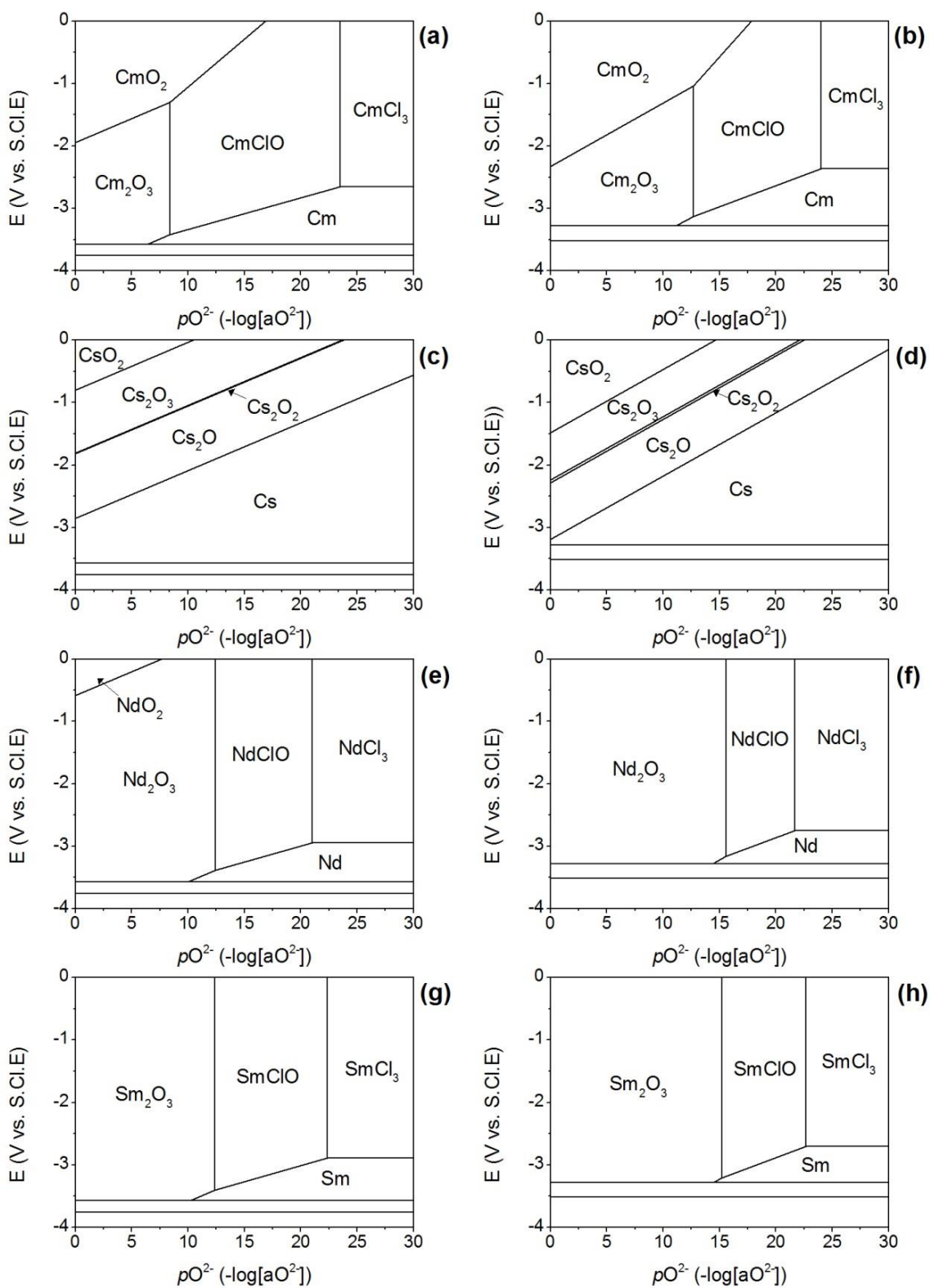


Figure 4. Predominance diagrams of (a) Cm, (c) Cs, (e) Nd, and (g) Sm in LiCl-KCl at 500 °C. (b) Cm, (d) Cs, (f) Nd, and (h) Sm are in NaCl-KCl at 750 °C

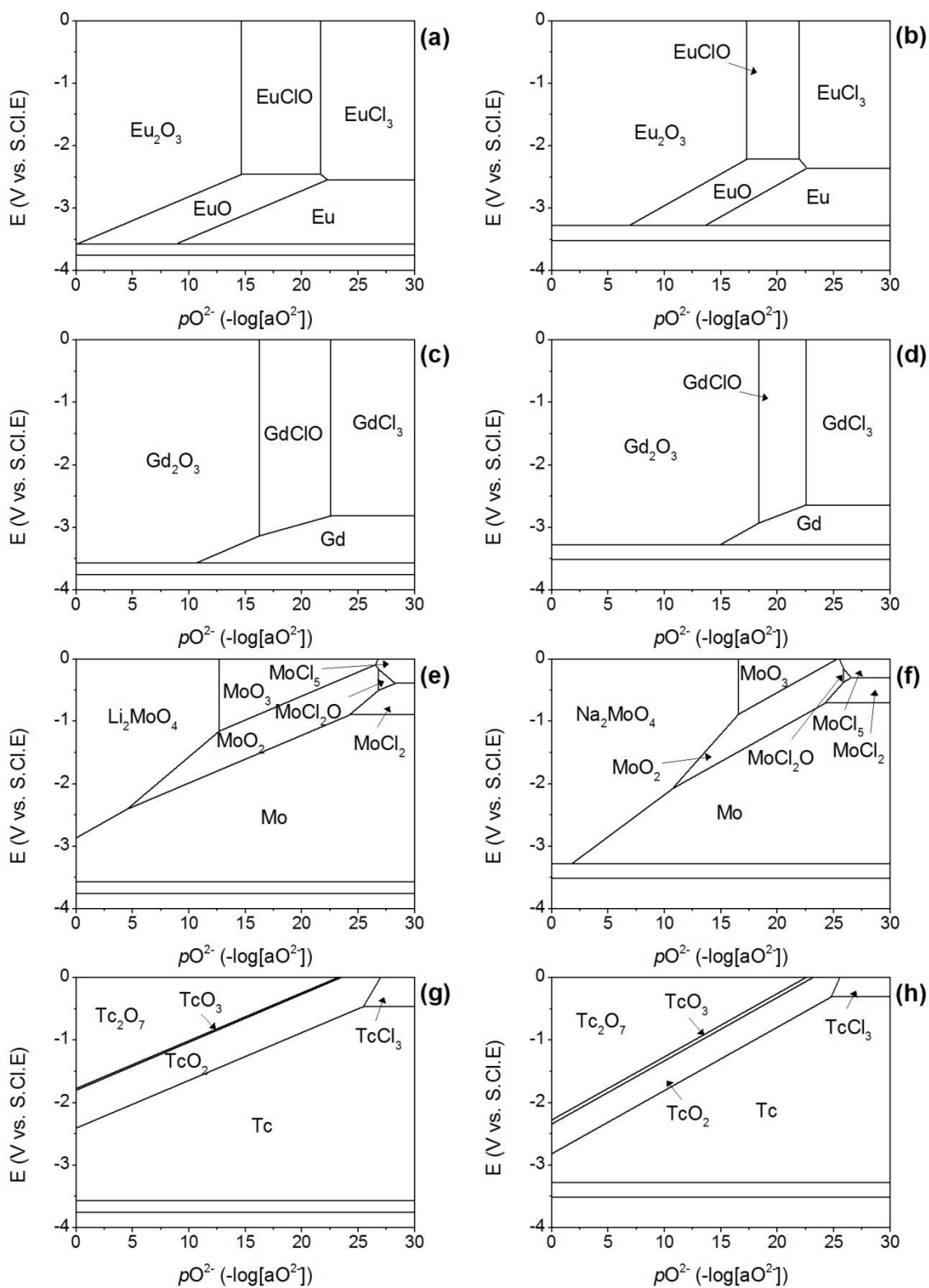


Figure 5. Predominance diagrams of (a) Eu, (c) Gd, (e) Mo, and (g) Tc in LiCl-KCl at 500 °C. (b) Eu, (d) Gd, (f) Mo, and (h) Tc are in NaCl-KCl at 750 °C

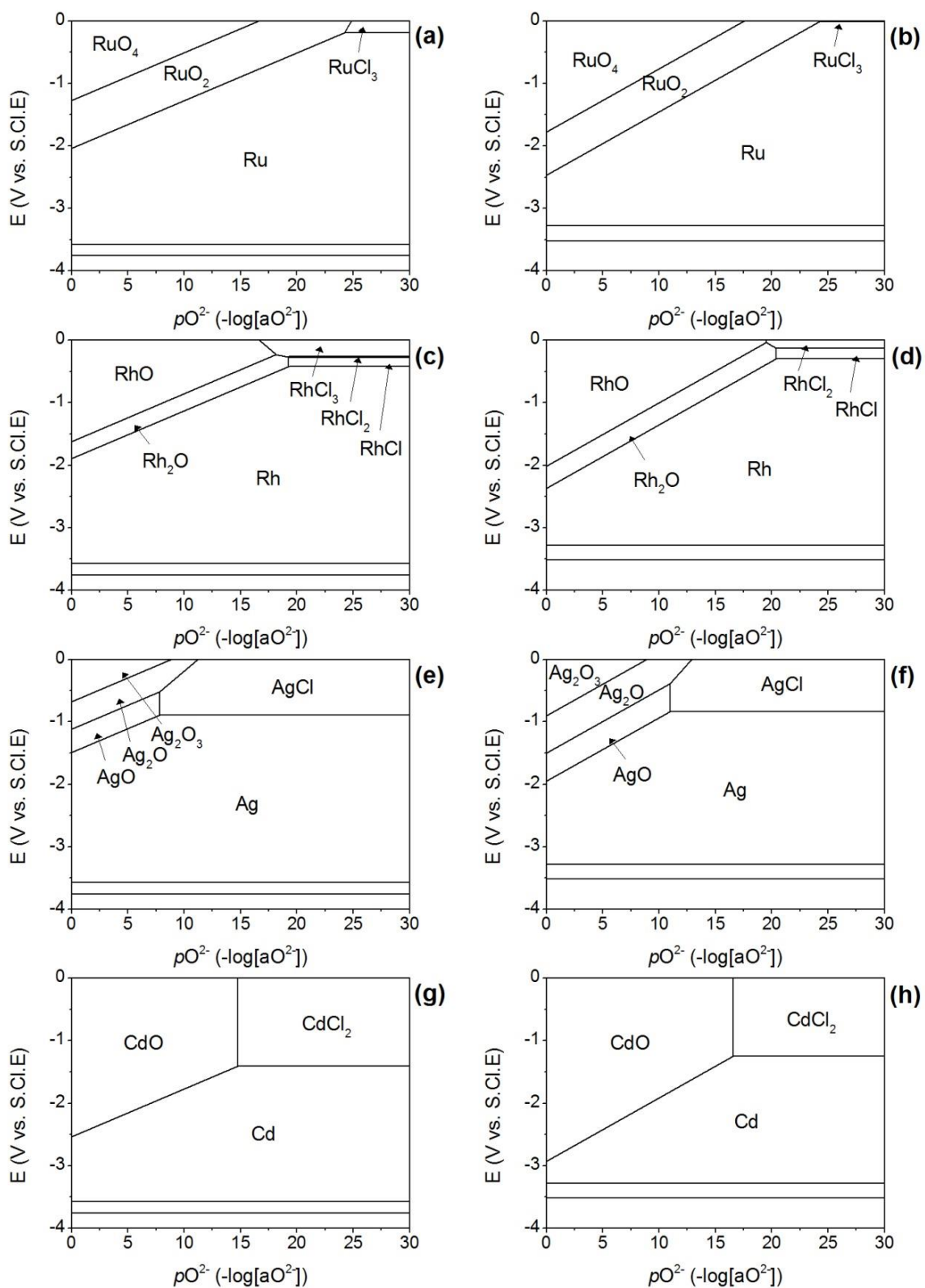


Figure 6. Predominance diagrams of (a) Ru, (c) Rh, (e) Ag, and (g) Cd in LiCl-KCl at 500 °C. (b) Ru, (d) Rh, (f) Ag, and (h) Cd are in NaCl-KCl at 750 °C

The predominance diagrams for U in NaCl-KCl, and for Pu, Np, Am, Cm, Cs, Nd, Sm, Eu, Gd, Mo, Tc, Ru, Rh, Ag and Cd, in both LiCl-KCl and NaCl-KCl, can be interpreted in the same way as for U in LiCl-KCl. They are all presented in Fig. 3-6 (a-h).

Temperature is an important parameter that affects the stability zones in the diagrams. At higher temperatures the regions of stability are shifted to the 'left', at higher O^{2-} activity, where oxide reduction reactions occur; however, at higher temperatures, the potential window is smaller.

4. DISCUSSION

The interface lines between the lowest oxidation state and the pure metal state are of particular importance for electrochemical reduction and pyroprocessing, for metal fuelled reactors; and the interface line between oxide states for oxide fuelled reactors. From Fig. 3-6, it is evident that the reduction of the transition metals, Rh, Ag, Ru, Tc, Cd and Mo, occurs first, at less negative potentials. Then, the reduction of U, Pu and the minor actinides, in the order of U, Cs, Pu, Am, Np and Cm at increasingly negative potentials. Finally, the reduction of the lanthanides in order of increasingly negative potential: Nd, Sm, Gd and Eu. These findings are encouraging, as the three different groups are clearly divided, thus indicating that they can be selectively reduced and separated from the spent-fuel. Separating Pu as a single species appears to be challenging, this is an important non-proliferation feature.

From Fig. 3-6, it is evident that some species have very narrow bands of stability, and thus might not be observed experimentally, if the metal oxides were to be reduced. This could be the case for U_3O_7 , UO, U_4O_9 , Np_2O_5 , Cs_2O_2 , $MoCl_2O$, TcO_3 and $RhCl_2$.

A predominance diagram for uranium species in LiCl-KCl has been produced [50]; however, this was based on stability values obtained from experimental results, and did not include the pure metal phase U, and the phases U_3O_8 , U_4O_9 and UCl_2O . The diagram produced here includes all these phases and is purely based on recent thermodynamic values. Predominance diagrams have also been published for the Pu and Am systems [51]. These are in agreement with the ones produced here in terms of stable phases, also the fact that the oxychloride phase in the Am system ($AmOCl$) is more stable than in the Pu system ($PuOCl$). Nonetheless, the values at which the interlines appear are somewhat different to here, this is due to the fact that the lines were calculated based on much lower ion activities than in this article. A more recent study [20] where the predominance diagram for the Pu system was established based on experimental results shows that the $PuOCl$ species is not stable at all. This is in contrast with the thermodynamically predicted results here. Predominance diagrams for the Cm system have also been published in 3LiCl-2KCl and NaCl-KCl [52], they show similar regions of stability to this work; however, the interface lines are shifted slightly. This is due to the fact that some of the values obtained were experimental as well. A diagram for Sm species in LiCl-KCl eutectic has also been published [53]. It shows the same regions of stability as the diagram here; nonetheless, the equilibrium lines are shifted again due to the use of different ion activities between Sm (II) and Sm (III). None of the other spent nuclear material species presented here have published predominance

diagrams (as known to the authors); however, many diagrams have been published for other materials in molten salts; such as for Ce and Fe [54], Cr [55] and Zr [26].

4.1. Comparison of eutectics

It is noticeable from Fig 3-6 that for all spent fuel materials, the region of stability for the pure metal phase is larger in the LiCl-KCl eutectic, than in the NaCl-KCl eutectic, even though the temperature is lower, 500 °C and 750 °C respectively. The final reduction stage from oxide to metal also appears to be possible at higher O^{2-} ion activities in LiCl-KCl compared to NaCl-KCl. Thus, it seems that the use of LiCl-KCl for molten salt pyroprocessing is more favourable than NaCl-KCl. However, this is purely based on thermodynamics and higher temperatures will benefit from faster kinetics.

4.2. Selective electro-reduction

Selective direct reduction is when there is a mixture of different metal oxides and only one, or a subset of them, are selectively reduced and separated via electroplating. This can be very beneficial in the nuclear industry, to enable the reprocessing and recycling of the useful spent fuel products selectively and separately, and also prevents nuclear proliferation. Thus, it is important to understand how control of electrode potential affects spent fuel products in a molten salt reprocessing reactor; comprehensive predominance diagrams are a starting point for such analyses.

One instance where the possibility of selective electro-reduction is not desired is for U and Pu. This is for anti-proliferation reasons. The predominance diagrams for Pu are superimposed onto those for U, in LiCl-KCl and NaCl-KCl, in Fig. 7. The main region of interest is the interface lines where the reduction from the lowest oxide state to the pure metal phase occurs. As seen in Fig. 7, these boundary lines for the U and the Pu systems are very close to each other. Thus, it would be challenging to selectively reduce one of them exclusively. From Fig. 7, it is evident that the uranium oxide reduction to uranium metal would occur first.

In principle, the use of predominance diagrams to aid the understanding of the feasibility of selective electro-reduction can be applied to all spent-fuel products, in order to understand the reduction procedure that they would undergo if they were all placed in a molten salt reprocessing reactor.

Within each group, transition metals, actinides and lanthanides, difficulties are apparent in the partial reduction of a single species. In the transition metals group, partial reduction is most likely to be achieved, with the exception of Cd and Mo, as their reduction interlines are too close to each other. In the actinides group, it is more difficult to perform partial reduction, Np being the exception. It is the most difficult to carry out partial direct reductions in the lanthanides group.

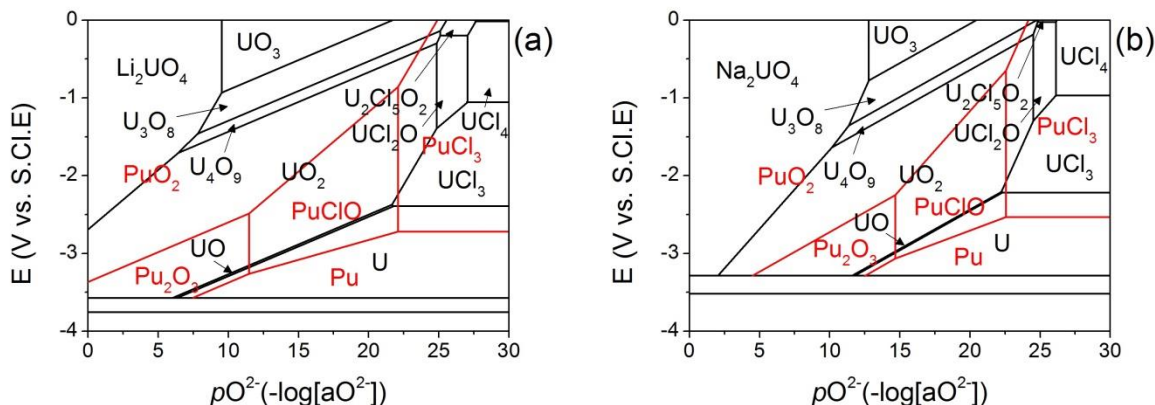


Figure 7. Predominance diagrams of U and Pu species. (a) in LiCl-KCl at 500 °C, (b) in NaCl-KCl at 750 °C

An example of where selective direct reduction would be useful is for Am and Cm: this is to mimic the EXAm process in solvent extraction nuclear reprocessing. Am and Cm are both high heat emitters; however, Cm has a short half-life, ~ 18 years, and thus, it is not economically viable to reprocess it. By contrast, it is desirable to reprocess and recycle Am. The predominance diagrams for Cm are superimposed onto those for Am, in LiCl-KCl and NaCl-KCl, in Fig. 8. From the predominance diagrams, it is evident that selective electro-reduction would be difficult for these two species due to the similarity in reduction potential. However, in this instance, the use of NaCl-KCl eutectic melt as the electrolyte is more favourable as the potentials for reduction of the two species form a larger window.

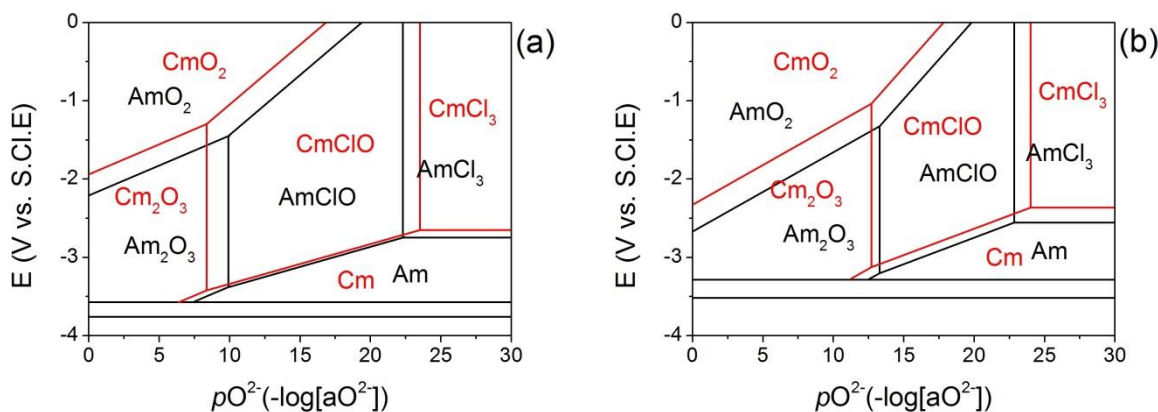


Figure 8. Predominance diagrams of Am and Cm species. (a) in LiCl-KCl at 500 °C, (b) in NaCl-KCl at 750 °C

5. CONCLUSIONS

Predominance diagrams are useful tools for understanding the electrochemistry and phase stability of metal-oxide systems in molten salts. They help in predicting experimental results and give

a good indication of whether an electrochemical process is thermodynamically feasible. For the first time, known to the authors, predominance diagrams have been generated for the range of spent nuclear fuel materials, based on established thermodynamic properties of the materials published in the literature.

By superimposing the diagrams for U and Pu, and Am and Cm onto each other, the potential for selective electro-reduction can be determined and the most suitable molten salt and temperature selected. It was found that molten salt pyroprocessing provides a promising route for reprocessing nuclear materials, which is also proliferation resistant. However, the approach is not seen to be a replacement for the EXAm process, as the selective reduction and separation of Am species from Cm would be challenging due to similarity in reduction potential.

ACKNOWLEDGEMENTS

This work was carried out as part of the UK Engineering and Physical Sciences Research Council (EPSRC) funded REFINE consortium (<http://www.refine.eng.ed.ac.uk/>) and EPSRC PACIFIC programme. We gratefully acknowledge financial support from the EPSRC (EP/J000531/1, EP/L018616/1, EP/M014371/1). Shearing acknowledges financial support from the Royal Academy of Engineering.

References

1. C. H. Poinssot, S. Bourg, N. Ouvrier, N. Combernoux, C. Rostaing, M. Vergas-Gonzalez and J. Bruno, *Energy*, 69 (2014) 199
2. NEA, *Pyrochemical separations in nuclear applications*, OECD, Paris (2014)
3. G. J. Lumetta, K. L. Nash, S. B. Clark and J. I. Friese, *Separations for the Nuclear Fuel Cycle in the 21st Century*, American Chemical Society (2006)
4. M. Iizuka, T. Koyama, N. Kondo, R. Fujita and H. Tanaka, *J. Nucl. Mater.*, 247 (1997) 183
5. T. Koyama, M. Iizuka, N. Kondo, R. Fujita and H. Tanaka, *J. Nucl. Mater.*, 247 (1997) 227
6. S. A. Kuznetsov and M. Gaune-Escard, *Electrochim. Acta*, 46 (2001) 1101
7. P. Masset, R. J. M. Konings, R. Malmbeck, J. Serp and J. P. Glatz JP, *J. Nucl. Mater.*, 344 (2005) 173
8. D. Lambertin, J. Lacquement, S. Sanchez and G. S. Picard GS, *Plasma & Ions*, 3 (2000) 65
9. D. Lambertin, J. Lacquement, S. Sanchez and G. S. Picard GS, *Electrochem. Commun.*, 4 (2002) 447
10. R. Littlewood, *J. Electrochem. Soc.*, 109 (1962) 525
11. M. Pourbaix, *Thermodynamics of Dilute Aqueous Solutions*, E. Arnold & Co, London (1949)
12. K. Dring, R. Dashwood and D. Inman, *J. Electrochem. Soc.*, 152 (2005) D184
13. L. D. Brown, R. Abdulaziz, S. Simons, D. Inman, D. J. L. Brett and P. R. Shearing PR, *J. Appl. Electrochem.*, 43 (2013) 1235
14. D. Inman and N. S. Wrench NS, *Brit. Corros. J.*, 1 (1966) 246
15. A. Conte and M. D. Ingram, *Electrochim. Acta*, 13 (1968) 1551
16. G. Picard, F. Seon and B. Trémillon B, *J. Electrochem. Soc.*, 129 (1982) 1450
17. T. H. Okabe and Y. Waseda, *JOM*, 49 (1997) 28
18. A. M. Martinez, Y. Castrillejo, E. Barrado, G. M. Haarberg and G. Picard, *J. Electroanal. Chem.*, 449 (1998) 67
19. T. Abiko, I. Park and T. H. Okabe, *Proceedings of the 10th World Conference on Titanium* (2003) 253
20. C. Caravaca, A. Laplace, J. Vermeulen and J. Lacquement, *J. Nucl. Mater.*, 377 (2008) 340

21. X. Y. Yan and D. J. Fray, *J. Appl. Electrochem.*, 39 (2009) 1349
22. G. Z. Chen, D. J. Fray and T. W. Farthing, *Nature*, 407 (2000) 361
23. C. Schwandt and D. J. Fray, *Electrochim. Acta*, 51 (2005) 66
24. S. Wang and Y. Li, *J. Electroanal. Chem.*, 571 (2004) 37
25. R. Bhagat, D. Dye, S. L. Raghunathan, R. J. Talling, D. Inman, B. K. Jackson, K. K. Rao and R. J. Dashwood, *Acta Mater.*, 58 (2010) 5057
26. V. Smolenski, A. Laplace and J. Lacquement, *J. Electrochem. Soc.*, 151 (2004) E302
27. R. Abdulaziz, L. D. Brown, D. Inman, S. Simons, P. R. Shearing and D. J. L. Brett, *Electrochem. Commun.*, 41 (2014) 44
28. NEA, *Spent Nuclear Fuel Assay Data for Isotopic Validation*, OECD, Paris (2011)
29. B. Trémillon, *Reactions in Solution: An Applied Analytical Approach*, John Wiley & Sons, New York (1997)
30. G. Radulescu, D. E. Mueller and J. C. Wagner, *Nucl. Technol.*, 167 (2009) 268
31. I. Barin, *Thermodynamic Data of Pure Substances*, VCH Verlags Gesellschaft, Weinheim (1993)
32. M. W. Chase, *JANAF Thermodynamic Tables*, American Institute of Physics, New York (1985)
33. Landolt-Bornstein, *Thermodynamic Properties of Inorganic Materials*, Springer Verlag, Berlin-Heidelberg (1999)
34. V. Glushko, *Thermocenter of the Russian Academy of Sciences*, IVTAN Association, Izhorskaya (1994)
35. Landolt-Bornstein, *Thermodynamic Properties of Inorganic Materials*, Springer Verlag, Berlin-Heidelberg (2001)
36. I. Barin, *Thermodynamic Data of Pure Substances*, VCH Verlags Gesellschaft, Weinheim (1989)
37. O. Knacke, O. Kubaschewski and K. Hesselmann, *Thermodynamic Properties of Inorganic Substances*, Springer Verlag, Düsseldorf (1991)
38. M. Binnewies and E. Milke, *Thermochemical Data of Elements and Compounds*, Wiley-VCH Verlag, Weinheim (2002)
39. D. G. Archera, *J. Phys. Chem. Ref. Data*, 28 (1999) 1
40. I. Barin, *Thermodynamic Data of Pure Substances*, VCH Verlags Gesellschaft, Weinheim (1995)
41. NEA, R. Guillaumont and F. J. Mompean, *Update on the Chemical Thermodynamics of Uranium, Neptunium, Plutonium, Americium and Technetium*, Elsevier, Amsterdam (2003)
42. L. P. Ruzinov and B. S. Gulyanitskii, *Equilibrium Transformations of Metallurgical Reactions*, Metallurgiya, Moscow (1975)
43. I. Barin, *Thermodynamic Data of Pure Substances*, VCH Verlags Gesellschaft, Weinheim (1977)
44. Landolt-Bornstein, *Thermodynamic Properties of Inorganic Materials*, Springer Verlag, Berlin-Heidelberg (2000)
45. A. J. Bard, R. Parsons and J. Jordan, *Standard Potentials in Aqueous Solution*, CRC press, New York (1985)
46. M. K. Karapet'iants and M. L. Karapet'iants, *Thermodynamic Constants of Inorganic and Organic Compounds*, Humphrey Science Publishers, New York (1970)
47. J. R. Haas, E. L. Shock and D. C. Sassani, *Geochim. Cosmochim. Acta*, 59 (1995) 4329
48. L. B. Pankratz, *Thermodynamic Properties of Carbides, Nitrides and Other Selected Substances*, U.S. Dept. of the Interior, United States Bureau of Mines, Washington, D.C. (1994)
49. M. W. Chase, *NIST-JANAF Thermodynamical Tables*, American Institute of Physics, New York (1998)
50. I. Uchida, J. Nikura and S. Toshima, *J. Electroanal. Chem.*, 124 (1981) 165
51. M. Akabori, H. Hayashi and K. Minato, *JAERI Conf.*, 007 (2005) 186
52. A. Osipenko, A. Mayershin, V. Smolenski, A. Novoselova and M. Kormilitsyn, *Electrochemistry of Curium in Molten Chlorides*, INTECH Open Access Publisher (2012)
53. G. De Cordoba and C. Caravaca, *J. Phys. Chem. Solids*, 67 (2006) 1862

54. T. Yamamura, M. Mehmood, H. Maekawa and Y. Sato, *Chem. Sustainable Development*, 12 (2004) 105
55. T. Ishitsuka and K. Nose, *Corros. Sci.*, 44 (2002) 247

© 2016 The Authors. Published by ESG (www.electrochemsci.org). This article is an open access article distributed under the terms and conditions of the Creative Commons Attribution license (<http://creativecommons.org/licenses/by/4.0/>).